Environmental Science Nano

ROYAL SOCIETY OF CHEMISTRY

PAPER

View Article Online
View Journal | View Issue

Cite this: *Environ. Sci.: Nano*, 2024, **11**, 406

Clearance of nanoparticles from blood: effects of hydrodynamic size and surface coatings†

Bingqing Lu,* Jiaqi Wang, A. Jan Hendriks and Tom M. Nolte

The distribution of nanoparticles (NPs) in the human body is associated with the development of nanomedicines and nanotoxicity. Physiologically based pharmacokinetic (PBPK) tools can simulate the distribution and elimination of NPs but are primarily dependent on experimental data. Models involving NP size and surface coating as parameters for estimating the clearance of NPs from blood are beneficial to the extension application of PBPK models. To this end, we first collected intravenous kinetic data on the blood distribution of 19 types of NPs for model parameterization and then collected 20 types of NPs for validation. Rate constants for clearance from blood were obtained by fitting the collected data to one- and two-compartment kinetics. A generic model (NP size-based) for estimation of rate constants was developed based on collision and diffusion behavior driven by NP size. NPs with a hydrodynamic diameter of 20 nm have the highest clearance rate constant *via* penetration and phagocytosis pathways. An extended model (NP size- and surface coating-based) was built to estimate rate constants of various NPs by calculating van der Waals energy between NPs and macrophages. Nearly 3/4 of the validation data are within 95% confidence intervals, indicating that our generic and extended models can be applied to NPs with different sizes and surface modifications.

Received 10th November 2023,
Accepted 7th December 2023

DOI: 10.1039/d3en00812f

rsc.li/es-nano

Environmental significance

The peer-reviewed literature contains fundamental methods for estimating the bioaccumulation of various nanoparticles based on possible pathways of elimination in the blood, covering particle size and particle surface coating properties. Our study expects to break the bottleneck that the current physiologically based pharmacokinetic model is difficult to extend to other particles, and contribute to the risk assessment of different nanoparticles or development of nanomedicines in humans.

1. Introduction

Nanoparticles (NPs) have a wide range of applications in various fields due to their unique properties (*e.g.*, small size, large surface area, and surface functionalization). Intentional exposure of organisms to NPs applies to medicine, including drug delivery,[1] medical imaging,[2] and disease diagnosis.[3] For example, NPs can facilitate targeted delivery of pharmaceuticals to tumors[4] in the brain by crossing the blood–brain barrier.[5] Non-targeted or environmental exposures may occur due to contact between NPs and the human skin[6] or respiratory tract.[7] NPs have wider biological effects after entering the bloodstream.[8] Trapping of NPs by the reticuloendothelial system in the immune system may lead to ineffectiveness of targeted NPs or increase the potential toxicity[9] of non-targeted NPs.[10,11] Consequently, it is important to quantify the influence of NP properties on the clearance of NPs from blood to optimize biomedical applications of targeted NPs and minimize toxicity of non-targeted NPs.

The elimination of NPs *in vivo* is often predicted using physiologically based pharmacokinetic (PBPK) tools.[12] In the last decades, more than 25 different nano-PBPK models have been developed,[13,14] covering metallic,[15–18] carbon,[19] quantum dots (QD),[20] liposome,[21] polymer[22] and crystal NPs.[23] Many types of NPs exist. However, the PBPK models have been calibrated on experimental data for a few particles only,[24,25] limiting application to broader classes of NPs. As an alternative, statistical methods are applied to estimate parameters of PBPK models[22] using the so-called quantitative structure–activity relationships (QSARs).[26] Unfortunately, connecting these statistical models to mechanisms is

Department of Environmental Science, Institute for Biological and Environmental Sciences, Radboud University Nijmegen, Nijmegen, 6500 GL, The Netherlands. E-mail: bingqing.lu@ru.nl

† Electronic supplementary information (ESI) available. See DOI: https://doi.org/10.1039/d3en00812f

difficult. In addition, overfitting may occur.[27] Hence, a generic approach for estimation of PBPK parameters based on NPs and tissue properties is urgently needed.

Size influences the behavior of NPs and clearance mechanisms in the blood. Small NPs are widely distributed into different organs by penetration or diffusion from the blood *via* the endothelial pores.[28] Extravasation of NPs into some critical organs (*e.g.*, brain)[29] is restricted due to tight junctions formed between the continuous endothelial cells. Pores of the inter-endothelial cell junction openings for non-fenestrated blood capillaries in lungs, skin and intestinal mesentery have sizes of approximately 5 nm.[30] NP penetration to the kidney also facilitates their clearance from blood. The glomerular epithelial (fenestrated) filtration slit is 12.1–15 nm in general,[31,32] and 5.5 nm (ref. 33) specifically for spherical quantum dots. Pores between sinusoidal endothelial cells (fenestrated) of the liver are larger (upper limit of pore size: 280 nm in rodents and 180 nm in humans),[32] permitting hepatocytes[34] to take up NPs and excrete NPs into the digestive system.

NPs ($d < 1$ μm) have various clearance pathways from blood, including permeation through sinusoidal pores (d <150–200 nm),[35] phagocytosis[35,36] by phagocytes in capillaries and transcytosis by vascular endothelial cells into the interstitium.[37] Li *et al.*[38] reported that a NP with a mean diameter of approximately 100 nm shows prolonged blood circulation. Cellular uptake into nonphagocytic cells depends on NP size, with an uptake optimum NP diameter of approximately 50 nm.[39] Multipath clearance prevents models from quantitatively describing the effect of NP size on NP clearance. Large NPs with a diameter >1 μm are cleared by the reticuloendothelial system[40] or filtered by lungs, liver, or spleen[41] from the blood because size-dependent momentum forces increase collision probability with the mononuclear phagocytic system.[41] By contrast, if the particle size is within 20 and 1000 nm,[41,42] physical clearance mechanisms are minimized, and circulation time is prolonged.

Surface coatings moderate the effects of size on clearance. The circulation time of NPs in the blood can be prolonged by hydrophilic modification. Polyethylene glycol (PEG) and analogues[43] were used as coatings of NPs to prevent interactions with plasma proteins[44] or the reticuloendothelial system. The absence of 'sufficient' chain density of PEG, *i.e.*, decreased hydrophilicity, aids opsonins to bind to the NP surface.[45] However, excessively high PEG density limits mobility and produces steric hindrance effects.[41,46] The length and surface density of PEG chains for 'shielding' depend on dosing requirements. Hoshyar *et al.*[47] showed that pegylation of small NPs increases their half-lives in blood. The mixed effects of NP size and surface coating on NP clearance behavior need to be considered.

Whereas the aforementioned studies shed valuable qualitative insight into biodistribution pathways and kinetics of NPs within the body, quantitative predictions are still lacking. This hampers the parameterization of PBPK models to be applied to many different NP types. In the present study, we aimed to quantify the clearance of NPs from blood involving two pathways: 1) NP penetration through capillary pores and 2) phagocytosis by macrophages located in capillaries between blood and tissues. The easily accessible parameter-size was used to build a generic model based on penetration and phagocytosis for estimating rate constants of clearance. The interactions between NPs and capillary pores/macrophages were modelled based on physical diffusion and collision. In addition, we expanded the phagocytosis-based model by adding surface coatings of NPs as parameters, detailing the interaction of NPs with macrophages, and expect to estimate the rate constants for clearance of various NPs in blood.

2. Methods

2.1. Data collection and analysis

We conducted an extensive literature search on Web of Science by using 'nanoparticles distribution in blood', 'biodistribution of nanoparticles *in vivo*', 'intravenous', 'nanoparticles' and 'physiologically based pharmacokinetic (PBPK)' as keywords to first obtain blood clearance kinetics of 19 data points for model parameterization and then collected 20 data points for model validation (16 data points for validating the generic model and four data points for validating the extended model). The data were to meet the following criteria: 1) spherical NPs are injected intravenously into different rats or mice as a single dose. 2) For parameterization we only used hydrodynamic sizes (measured by dynamic light scattering (DLS)), whereas for validation we used both TEM (transmission electron microscopy) sizes and hydrodynamic sizes. 3) NPs are coated by the same chain of compounds instead of multiple chains with compounds (*i.e.*, mixed coatings). 4) At least four data points of NP concentration were measured over time. 5) Rate constants for clearance of NPs from blood were obtained with statistical significance ($p < 0.05$). The sources (studies), materials, properties and conditions of test animals of all data for parameterization and validation are shown in Table 1. All NP diameters range from 2 to 220 nm.

All pharmacokinetic data were fitted to one-compartment ($C(t) = C(0)\cdot e^{-kt} + C(\infty)$) and two-compartment pharmacokinetic models ($C(t) = C_c(0)\cdot e^{-k_c t} + C_p(0)\cdot e^{-k_p t}$). The two-compartment kinetic model assumed that the distribution of NPs in the central compartment (arterial blood and highly perfused tissues including kidneys and liver) is practically instantaneous compared to the distribution of NPs in the peripheral compartment (poorly perfused tissues such as muscles). Results for kinetic fits are given in Fig. S1 and Table S1 in the ESI.† 95% confidence intervals of all models were calculated as described previously.[48]

2.2. Prediction of rate constants for clearance of NPs from blood

2.2.1 Clearance pathways. Clearance of NPs from blood may involve penetration of NPs from capillary pores into tissues (*e.g.*, interstitial)[25,71] and cellular uptake by phagocytes for large NPs. Fig. 1 shows the two main clearance pathways for NPs after intravenous injection. NPs can flow back to the heart from veins after injection and then flow to different tissues (*e.g.*, central

Table 1 The modifications of NPs and conditions of experimental animals for data used in parameterization and validation (only unhealthy mice/rats are marked)

NP-core-coatings	Sizes (nm)	Zeta potential (mV)	Animal/health
Data for parameterization			
QDPEG5000/2000 (ref. 49)	15.5[b]	—	Mice
QD-CdTe/CdS[25]	4.2[b]	—	Mice
PAMAM CND[50]	5[b]	+2.5	Mice with melanoma
PAMAM CND[50]	11[b]	−20	Mice with melanoma
$Cu_{2-x}Se$ NP[51]	5.6[b]	—	Mice
CdTe-QD[52]	4.0[b]	—	Mice
AuNP[53]	2.0[b]	—	Mice
ZnO[18]	10[b]	−27.1	Mice
ZnO[18]	71[b]	−19.3	Mice
IONPs-PEG2000 (ref. 54)	26.5[b]	—	Mice
IONPs-PEG5000 (ref. 54)	34.2[b]	—	Mice
IONPs- PEG5000 (ref. 54)	81[b]	—	Mice
PLGA-mPEG256-5000 (ref. 55)	114.8[b]	−6.2	Mice
PLGA-mPEG153-5000 (ref. 55)	97.4[b]	−5.9	Mice
PLGA-mPEG61-5000 (ref. 55)	79[b]	−4.7	Mice
PLGA-mPEG34-5000 (ref. 55)	67[b]	−5.2	Mice
PAA(Polyacrylamide)[56]	31[b]	—	Rat
PAA-PEG[56]	35[b]	—	Rat
Nanocrystal[23]	203[b]	—	Rat
Data for validation			
AuNP-PEG5000 (ref. 57)	4[a,c]	—	Mice
AuNP-PEG5000 (ref. 57)	13[a,c]	—	Mice
QD705-PEG5000 (ref. 58)	13[c]	—	Mice
QD705-PEG5000 (ref. 58)	18.5[c]	—	Mice
AuNP-PEG[59]	88.9[b]	−27.1	Tumor-bearing mice
AuNP-PEG[60]	38[b]	−10.5	Mice
AuNP-Trimethylammonium groups and sulfonic groups[60]	20[b]	−9.8	Mice
AuNP-Citric acid-PEG-Thioctic acid[61]	45.4[b]	−7.4	Mice
AuNP-Citric acid-PEG-Thioctic acid[61]	60[b]	−7.4	Mice
AuNP-Citric acid-PEG-Thioctic acid[61]	89.3[b]	−9.4	Mice
AuNP-Dextran[62]	46[b]	—	Athymic nude mice
Graphene oxide-PEG-NH2,p-SCN-Bn-NOTA[d63]	220[b]	+4	Mice bearing cbgLuc-MDA-MB-231 tumor nodules in lungs
64Cu-multifunctional mesoporous silica NP-800CW[e64]	175.3[b]	−3.3	Tumor-bearing mice
64Cu-NOTA-hollow mesoporous silica NP-ZW800-PEG-TRC105 (ref. 65)	194[b]	−5.1	Tumor-bearing mice
Cy5 dye-encapsulating core–shell silica NP[66]	7[b]	—	Athymic nude mice with human melanoma
IONPs-*N*-(trimethoxysilylpropyl)ethylenediaminetriacetate trisodium salt[67]	29[b]	−39	Mouse with blood–brain barrier disruption and under magnetic targeting
DL-Poly(L-lactide) NP[68]	187.7[b]	−37.7	Mice
PEG-Poly(L-lactide)-PEG NP[68]	171.5[b]	−2.2	Mice
Methoxy-PEG-poly(lactide-*co*-glycolide)-PEG-Methoxy (PELGE)[69]	100[c]	—	Mice
Yb_2O_3-Silanated m-PEG[70]	175[c]	−0.9	Mice

[a] Denotes pore sizes of AuNPs without coating. [b] Denotes hydrodynamic diameter based on DLS. [c] Denotes diameters based on TEM. [d] Denotes (*i.e.*, 2-*S*-(4-isothiocyanatobenzyl)-1,4,7-triacetic acid) and FSHR-mAb-SH. [e] Denotes (fluorescence dye)-human/murine chimeric IgG1 monoclonal antibody (TRC105). NPs used in the extended model are marked in bold.

compartments like the liver and kidney) *via* the aorta. Small NPs (smaller than pores) can penetrate membranes in the liver and glomeruli in the kidney *via* capillary pores, or can be excreted in urine. Large NPs tend to be taken up by phagocytes (*e.g.*, macrophages) primarily located in liver capillaries and intraglomerular mesangial cells in the kidney due to phagocytosis/micropinocytosis.[72]

2.2.2 Collision theory. Collision theory is widely used to describe the aggregation of particles, facilitating its applications in industry,[73] materials[74] and environmental science.[75] In the field of biology, collisions between particles and organisms (protein corona)[76] are also relevant. Here, collision theory is used to explore the interaction between NPs and pores in the penetration pathway, and interaction between NPs and macrophages in the phagocytosis pathway. The rate constant k based on collision theory[77] can be described as:

$$k = Z{\cdot}\rho{\cdot}e^{\frac{-E_a}{k_B T}} \quad (1)$$

where Z (s^{-1}) is the collision frequency in general. ρ is a steric factor (<1), a function of shape; $e^{-E_a/(k_B T)}$ is the thermodynamic effectivity of interaction, where E_a is the activation energy (J).

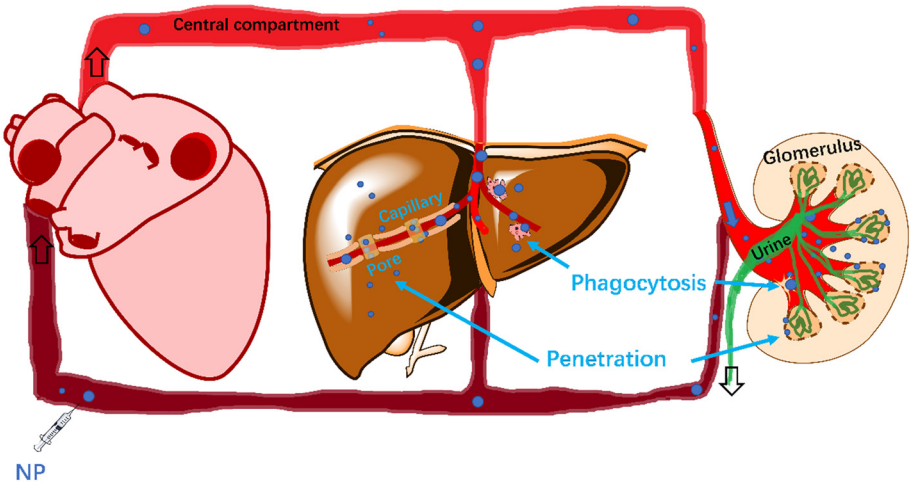

Fig. 1 Two clearance pathways for NPs injected intravenously. NPs circulate to different organs (*e.g.*, liver and kidney): 1) NPs can diffuse/penetrate through capillary pores into the liver and kidney (clearance from blood). Small NPs even pass through filtration slits into glomeruli after penetration from endothelial cells, and then be excreted from urine (clearance from the body). 2) NPs can be taken up by macrophages located in liver capillaries and intraglomerular mesangial cells.

2.2.3 Prediction of rate constant *k* (obtained by one-compartment) for clearance by the generic model. The generic model was built to predict the rate constant k for clearance, following both penetration and phagocytosis pathways. During pore penetration pathways, the interaction frequency of NPs and pores (Z_p, s^{-1}) can be deduced as[77]

$$Z_p = {}^{N_A\sigma_p}\sqrt{\frac{8k_BT}{\pi\mu_p}} \quad (2)$$

with N_A as Avogadro's constant, k_B as Boltzmann's constant and T as temperature (K). The interaction cross sectional area σ_p is calculated assuming that the whole NP interacts with(in) a pore. Penetration requires that the radius of the pore is larger than the NP radius r_{np}, hence, $\sigma_p = 4\pi r_{np}{}^2$. μ_p is the reduced mass of NPs and pores. Given that we aim to build a generic model that only considers spherical NPs and does not take into account the NP and pore density/mass, the parameters (ρ and μ_p) would be simplified. The influence of $e^{-E_a/(k_BT)}$ (in eqn (1)) was ignored as well for a generic model involving size as the only parameter. By setting θ to simplified terms $\left(N_A{\cdot}4\pi\sqrt{8k_BT/\left(\pi\mu_p\right)}{\cdot}\rho{\cdot}e^{-E_a/k_BT}\right)$ and filling θ in eqn (1) and (2), rate constants for clearance based on penetration pathways ($k_{penetration}$) could be

$$k_{penetration} = N_A{\cdot}4\pi r_{np}{}^2\sqrt{\frac{8k_BT}{\pi\mu_p}}{\cdot}\rho{\cdot}e^{\frac{-E_a}{k_BT}} = \theta{\cdot}r_{np}{}^2 \quad (3)$$

Clearance of NPs by the reticuloendothelial system depends on interaction between NPs and phagocytes (*i.e.*, macrophages). Encounters between NPs and the macrophages may trap NPs, influencing clearance rates of NPs in the blood. According to collision theory, the frequency of encounters between NPs and macrophages (Z_m, s^{-1}) in aqueous solutions is[78]

$$Z_m = 4\pi RD_r \quad (4)$$

where R is the sum of r_{np} and the radius of macrophage r_m (macrophages utilize two types of motilities, amoeboid and mesenchymal;[79] however, our generic model does not consider deformation of macrophages), describing the radius of the collision cross-section (m). D_r is the relative diffusion constant between NPs and macrophages ($m^2\ s^{-1}$) with $D_r = D_{np} + D_m$,[78] where D_{np} is the diffusion constant of NPs and D_m is the diffusion constant of macrophages. Collisions in liquids are generally based on the Stokes–Einstein relation,[80,81] defined as

$$D_r = D_{np} + D_m = \frac{k_BT}{6\pi\eta}{\cdot}\left(\frac{r_{np}+r_m}{r_{np}{\cdot}r_m}\right) \quad (5)$$

where η is the dynamic viscosity of blood. Plugging eqn (4) and (5) into eqn (1), the clearance rate constant $k_{phagocytosis}$ equals

$$k_{phagocytosis} = \rho{\cdot}4\pi\frac{\left(r_{np}+r_m\right)^2}{r_{np}{\cdot}r_m}{\cdot}\frac{k_BT}{6\pi\eta}{\cdot}e^{\frac{-E_a}{k_BT}} \quad (6)$$

The parameters ρ, η and $e^{-E_a/(k_BT)}$, related to hydrophobicity or surface energies of NPs, were merged into a simplified term 'α' since all NPs share the same environmental conditions in organisms and the generic model does not consider surface energies. We set the average radius of macrophages r_m to 21/2 = 10.5 μm.[48] Thus, eqn (6) simplifies to:

$$k_{phagocytosis} = \alpha{\cdot}\frac{\left(r_{np}+r_m\right)^2}{r_{np}{\cdot}r_m} \quad (7)$$

To our knowledge, there are no experimentally derived values for θ and α published in the literature. However, the relationship between the rate constant k and radius of NPs allows extracting the universal θ and α for all collected NP datasets. NPs can be eliminated by different pathways, resulting in total clearance of NPs from blood. The total rate constant k

for clearance of NPs from blood can be obtained by assuming that underling mechanisms (penetration and phagocytosis) operate in parallel (ESI† Methods 1.1 and Fig. S2). The total rate constant k for clearance is thus $\left(\frac{1}{k}=\frac{1}{k_{\text{penetration}}}+\frac{1}{k_{\text{phagocytosis}}}\right)$ described generically as:

$$k=\frac{k_{\text{penetration}}\cdot k_{\text{phagocytosis}}}{k_{\text{penetration}}+k_{\text{phagocytosis}}}=\frac{\theta\cdot {r_{\text{np}}}^2\cdot\alpha\cdot\frac{\left(r_{\text{np}}+r_{\text{m}}\right)^2}{r_{\text{np}}\cdot r_{\text{m}}}}{\theta\cdot {r_{\text{np}}}^2+\alpha\cdot\frac{\left(r_{\text{np}}+r_{\text{m}}\right)^2}{r_{\text{np}}\cdot r_{\text{m}}}} \quad (8)$$

We therefore obtained θ and α *via* fitting experimentally derived values for k to the NP's hydrodynamic radius r_{np}.

2.2.4 Prediction of rate constant k_c (obtained from two-compartment) by the extended model. The clearance rate constants/half-lives of NPs are also affected by macrophage polarization.[82,83] NP surface coating could, for instance, influence the amount and type of opsonins, adsorption onto NP surfaces, macrophage uptake and, hence, clearance. Macrophages interact with NP surface coating which can be characterized by surface energies. Surface energies were shown to relate to hydrophobicity, as outlined in previous work.[48] We implemented a term $(e^{-E_a/(k_B\cdot T)})$ (eqn (6)) for statistical thermodynamics that uses van der Waals surface energies[27,84] of NP coatings expanding the generic phagocytosis-based model in the ESI.† In ESI† Methods 1.2, the van der Waals energy[73] ($\Delta G_{\text{LW}}(h)$), being part of the activation energy E_a ($E_a=\delta\cdot\Delta G_{\text{LW}}(h)$), was used to replace E_a. The van der Waals free energies of NPs (*e.g.*, the Lifshitz–van der Waals, ${\gamma_{\text{np}}}^{\text{LW}}$) and macrophages (${\gamma_{\text{m}}}^{\text{LW}}$) were calculated or collected to obtain the van der Waals energy (Eqn (S5†), $\Delta G_{\text{LW}}(h)$, h is the separation distance between the interacting surfaces). By using $\Delta G_{\text{LW}}(h)$ to replace E_a, eqn (6) can be transformed to the logarithmic form as

$$\ln(k_c)=\ln(Z_m)+\ln(\rho)+\delta\cdot\Delta G_{\text{LW}}(h) \quad (9)$$

where δ is the slope of the linear regression. The functions for calculating $\Delta G_{\text{LW}}(h)$ are all included in the ESI.† All symbols and definitions in the formulas are shown in Table 2.

3. Results and discussion

3.1. Fits for clearance rate constants of NPs in blood

All fitting profiles and results based on one- and two-compartment kinetics for 19 data with different NP types (on blood clearance) are shown in Fig. S1 and Table S1,† respectively. Most NPs fitted well into the one-compartment model. An exception was noted for PLGA-mPEG$_{153-5000}$ (p = 0.14). Besides, the statistical significance of three two-compartment fittings could not be calculated (two PAMAM CNDs and one CdTe-QD) because the number of data points is too small for a two-compartment kinetics with four parameters. Some two-compartment fittings (QDPEG$_{5000/2000}$, QD CdTe/CdS, IONPs-PEG$_{2000}$, PLGA-mPEG$_{256-5000}$ and PLGA-mPEG$_{61-5000}$) showed increasing blood concentrations over time due to

Table 2 Factors used in the equations with typical or default values for parameters

Symbol	Description	Unit	Typical or default value
C_0	Initial concentration of NP	$\mu(n)g\ g^{-1}(mL^{-1})$	—
C_c	Initial concentration of NP in central compartment	$\mu(n)g\ g^{-1}(mL^{-1})$	—
C_p	Initial concentration of NP in peripheral compartment	$\mu(n)g\ g^{-1}(mL^{-1})$	—
d	Diameter	nm	—
D_m	Diffusion constant of monocyte/macrophage	$m^2\ s^{-1}$	—
D_{np}	Diffusion constant of NP	$m^2\ s^{-1}$	—
D_r	Relative diffusion constant between NP and macrophage	$m^2\ s^{-1}$	—
E_a	Activation energy	J	—
h	Separation distance between the interacting surfaces	nm	0.157
k	Rate constant for clearance in one-compartment	h^{-1}	—
k_B	Boltzmann constant	$J\ K^{-1}$	1.38×10^{23}
k_c	Rate constant for clearance in central compartment	h^{-1}	—
k_p	Rate constant for clearance in peripheral compartment	h^{-1}	—
$k_{\text{penetration}}$	Rate constant for penetration	s^{-1}	—
$k_{\text{phagocytosis}}$	Rate constant for phagocytosis	s^{-1}	—
N_A	Avogadro constant	mol^{-1}	6.02×10^{23}
R	The sum of r_{np} and r_m	nm	—
r_m	Radius of macrophage	μm	10.5
r_{np}	Radius of NP	nm	—
T	Temperature	K	—
Z	Collision frequency in general	s^{-1}	—
Z_m	Collision frequency between NP and macrophage	s^{-1}	—
Z_p	Collision frequency between NP and pore	s^{-1}	—
$\Delta G_{\text{LW}}(h)$	van der Waals interaction energy	J	—
η	Dynamic viscosity of blood	$m^2\ s^{-1}$	—
μ_p	Reduced mass of NP	kg	—
ρ	Steric factor	Unitless	—
σ_p	Interaction cross section	nm^2	—
${\gamma_{\text{np}}}^{\text{LW}}$	van der Waals free energies of NP coatings	$J\ m^{-2}$	—
${\gamma_m}^{\text{LW}}$	van der Waals free energies of macrophage	$J\ m^{-2}$	30

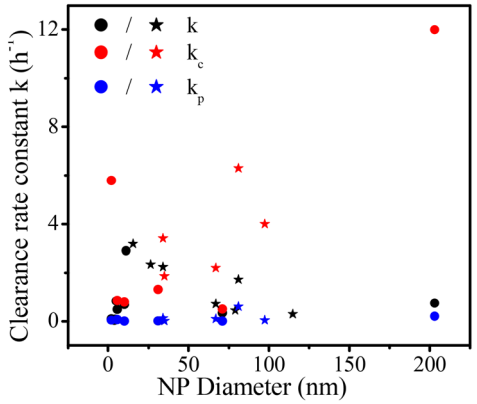

Fig. 2 Rate constants for clearance based on one- (k) and two-compartment (k_c and k_p) kinetics for pegylated NPs (stars) and non-pegylated NPs (dots) *versus* NP diameter.

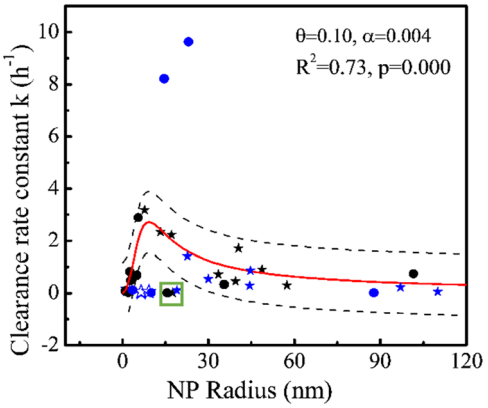

Fig. 3 Rate constant k (h^{-1}) for clearance based on one-compartment kinetics *versus* radius (nm) of NPs for pore penetration and phagocytosis with data on pegylated NPs (stars) and non-pegylated NPs (dots) for hydrodynamic size (solid) and TEM size (open). Black symbols denote 19 data points for parameterization and blue symbols denote 16 data points for validation. All symbols denote experimental data and the red curve was obtained using eqn (8). The dashed black lines show 95% confidence intervals of the model. The green square marks two overestimated outliers (black symbols) we did not involve in the regression.

equilibration or redistribution of NPs between tissues and the vascular system,[49] which is not captured by our model.

Fig. 2 shows all rate constants for clearance based on one- and two-compartment kinetics as a function of NP diameter. Most one-compartment rate constants k for clearance vary between the rate constants k_c and k_p based on two-compartment kinetics ($k_p < k < k_c$). The one-compartment parameter k (in black) seems to increase with NP size and then to decrease with increasing NP size. The distribution of k_c (in red) relative to the NP size is more variable than k, indicating that size is not the only factor affecting k_c. All two-compartment fittings show that the rate constants for clearance of the central compartment are greater than those of the peripheral compartment ($k_c \geq k_p$). The rate constants k_p (in blue) for clearance of the peripheral compartment for all NPs are close to zero.

Non-pegylated NPs (ZnO NP, 10 nm) have the lowest rate constant k_p (0.002) for clearance in the peripheral compartment, and the corresponding half-life is 346 hours. The most extended half-life is obtained for one non-pegylated NP (ZnO NP), opposite to the idea that pegylated NPs usually have long half-lives as the low surface hydrophobicity evades opsonin modification and reduces reticuloendothelial system capture.[45] Chen *et al.*[18] reported that a considerable number of ZnO NPs are captured by lung macrophages, increasing NP circulation time in pulmonary circulation. NPs that enter the lungs may travel from the interstitium to the lymphatic system[8] where they are likely re-released into the blood. These complex mechanisms may cause prolonged NP circulation time in blood. Besides, the solubility of ZnO NPs may also increase their blood circulation time because researchers took the concentration of (ref. 65) Zn as the concentration of ZnO NPs.[18]

3.2. Rate constants k for clearance (obtained from one-compartment kinetics) as a function of NP size

19 rate constants (Table 1) based on one-compartment were used to parameterize the generic model in Fig. 3 (black symbols). The generic model (NP size-based, obtained from eqn (8)) following penetration and phagocytosis mechanisms is shown in Fig. 3 (red curve). The rate constants k for clearance based on one-compartment kinetics were statistically significant related to the radius of NPs reflecting pore penetration and phagocytosis, proving that taking size as the only parameter could be used to estimate the rate constants k for clearance of NPs from blood.

Fig. 3 shows that rate constants k for clearance increase with increasing NP size when the NP's hydrodynamic diameter is smaller than ~20 nm, consistent with the penetration mechanism where $k_{penetration}$ increases with increasing NP size ($k_{penetration} \sim r_{np}^2$, eqn (3)). Our modeling is similar to the ratio ($\sim r_{np}^2$) of distribution of a solute between a pore and solutions.[85] By contrast, Fig. 3 also shows that rate constants k for clearance decrease with increasing NP size when the NP's hydrodynamic diameter is larger than ~20 nm, consistent with the phagocytosis mechanism where $k_{phagocytosis}$ decreases with increasing NP size ($k_{phagocytosis} \sim r_{np}^{-1}$, eqn (7)). According to the Stokes–Einstein relation, larger NPs are expected to be less mobile (the diffusion coefficient D_{np} is inversely proportional to the size, see Methods eqn (5)), resulting in fewer encounters between NPs and macrophages, and reducing phagocytosis.

The clearance of NPs from blood is the result of the dual action of penetration[25] and phagocytosis,[86] which is also the result of mutual restriction of NP collision and diffusion ability. The increased phase (NP from 0 to ~20 nm) of rate constants k with increasing NP size illustrates that penetration might contribute more than phagocytosis. At the same time, the slope changes from positive to negative as the particle size increases, which seems to indicate that phagocytosis becomes more dominant following the increase

of NP size. Penetration might contribute more than phagocytosis for clearance of smaller NPs for several reasons. Small NPs (for example, d = 18 nm) with strongly curved surfaces lead to protein interactions distinct from larger NPs (for example, d > 78 nm). Reduced opsonin attachment[41] increases pore penetration of small NPs and reduces recognition by macrophages.[87]

The highest rate constant k for clearance from blood occurs when the hydrodynamic diameter of the NP is around ~20 nm, which may imply that NP–pore/macrophage interactions *via* collision and diffusion are beneficial to each other. At this time, $k_{\text{penetration}}$ might equal $k_{\text{phagocytosis}}$. Generally, the clearance of NPs from blood includes the distribution of NPs from blood to organs and clearance of NPs from blood to urine (outside of the body) by glomerular filtration. We call the latter absolute clearance, since it is impossible for NPs to return from the urine to blood. Sizes of 10–20 nm (ref. 37 and 88) can rapidly be taken up by the liver and sizes of less than 5–15 (ref. 33 and 89) nm are more easily excreted through glomerular filtration,[31] which increase the clearance of NPs from blood. By contrast, NPs with sizes of 20–200 nm (ref. 41) can remain in circulation for an extended period, as confirmed by our modeling. The decreasing slope in Fig. 3 might not apply when the model covers larger NP sizes (to include micron sizes) due to other factors like gravitational pull,[41] which can be ignored for NPs. NP aggregation could also take place to increase cellular uptake,[90] which is not covered by our generic modeling and can be carried out in the future.

Clearly, our model is not perfect (R^2 = 0.73) as penetration and phagocytosis are the only pathways considered. To validate the model, we used 16 rate constants from studies not used for parameterization (four NPs with TEM size marked as open blue symbols and 12 NPs with hydrodynamic size marked as solid blue symbols in Fig. 3). Three of the four data points with only core size and TEM size (marked as open blue symbols in Fig. 3) are out of the generic model due to lack of well-defined hydrodynamic sizes. Their hydrodynamic behavior may render their penetrative capacity uncertain. Hydrodynamic sizes are usually larger than primary size due to hydration layers, electric double layers, and aggregation.[91] Besides, 8 of the 12 data points marked in solid blue symbols (Fig. 3) can be predicted well by our generic model because they are within 95% confidence intervals (dashed line in Fig. 3), which support that the generic model could provide generic prediction of various NPs. The model based on one parameter (radius of NPs) allows one to avoid overfitting. Two of the 12 data points (46 nm AuNP-Dextran and 29 nm IONPs) were greatly underestimated (k ~ 8–10 h^{-1}) and 2 of the 12 data points (38 nm AuNP-PEG and 20 nm AuNP-mixed groups) were overestimated by our model. The two overestimated data points came from the same study,[60] which might reflect specific conditions not covered by the model. The two underestimations (Fig. 3) were obtained from immunodeficient mice or mice with blood–brain barrier disruption under magnetic targeting, whereas 17 of the 19 data points for model parameterization were obtained from healthy animals. Although some studies reported that tumor-bearing does not significantly affect the overall biodistribution of NPs,[92,93] the influence of the disease on NP clearance from blood needs further research. In addition, surface charge[44] could influence NP behavior (*e.g.*, 29 nm IONPs are highly negative). The two data points (PAA-coated NP and PAA-PEG-coated NP, marked by a green square in Fig. 3) out of 95% confidence intervals confirm that other factors exist (*e.g.*, surface coatings, discussed in the later section). Other pathways not considered by our generic model could influence NP clearance behavior, causing prediction error, *e.g.*, clathrin-mediated internalization by endothelial cells.[94]

3.3. Rate constants k_c for clearance (obtained from two-compartment kinetics) as a function of NP size and surface coating

In our extended phagocytosis-based model (2.2.4), the van der Waals interaction energy ($\Delta G_{LW}(h)$) between NPs and macrophages was used to predict the rate constants k_c for clearance (eqn (9)). Seven out of the 19 data points for parameterization were used to build the extended model because of available information on surface coatings in Fig. 4 (black symbols). The linear regression (red line, eqn (9)) between van der Waals interaction energy $\Delta G_{LW}(h)$ and $\ln(k_c) - \ln(Z_m)$ is shown in Fig. 4. The regression is statistically significant with a high R^2 (0.95) and low p-value ((<0.0001)), indicating that interaction between macrophages and NPs drives the clearance of NPs in the well-perfused compartment (k_c). After involving properties of surface coatings, outliers in the generic model (marked in a green square in Fig. 3) fitted well to the extended model (Fig. 4), indicating that the behavior of some NPs in the blood can be affected by both NP size and surface coating.

Four independent data points are added (Tables S1 and S2†) to test the extended model and Fig. 4 shows that three out of the four data points are within the 95% confidence intervals (dashed line in Fig. 4). The prediction of NP coated by mPEG-PLA (Poly(L-lactide))-mPEG (PELE) copolymers with 30% PEG[68] is deeply lower than our estimation (Fig. 4). The surficial structure of PELE copolymers with 30% PEG was not reported in the original study, and the structure from work in ref. 95 was used, which may have caused deviations. Our current modeling does not consider the proportion of coatings, which might cause prediction errors. In addition, deviations in rate constants for clearance may be introduced by multiple interlaced data point lines in the original image. Interestingly, two tested data points with TEM size (170–190 nm) can be estimated well, illustrating that the function of size might be diluted by the effects of surface coatings in some scales. As the number of data is limited, more data is needed to increase the accuracy and precision of the model.

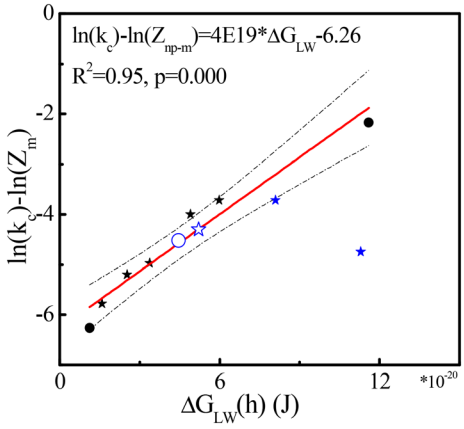

Fig. 4 $\ln(k_c) - \ln(Z_m)$ as a function of van der Waals interaction energy $\Delta G_{LW}(h)$ (J) for pegylated NPs (stars) and non-pegylated NPs (dots) with hydrodynamic size (solid) and TEM size (open). All symbols denote experimental data and the red line was obtained with eqn (9). The dashed black lines show 95% confidence intervals of the model. Blue symbols denote four tested data points (Table 1) from studies not used for parameterization.[68–70]

van der Waals energies explain the clearance kinetics of NPs in blood, *via* phagocytosis, as shown in Fig. 4. Indeed, van der Waals energies appear especially relevant for opsonin/macrophage interaction.[96] Particle/pathogen uptake involves macrophage polarization[97] and van der Waals energies are essential forces from induced dipoles: forces from polarization.[98] In addition, the coatings we used in current model show neutral or negative charges (Table 1). Surface charge[44] and targeting ligands[99] may affect opsonin adsorption as well, in turn affecting the clearance of NPs by phagocytosis. Our model might be extended in the future to include more interaction energies, such as electrostatic energy[100] and binding energy of ligands and receptors,[101] to explore the effect of net positive surface charges and ligand modification on NP accumulation[102] or clearance in the body. In addition, the clearance of NPs in peripheral compartments (*e.g.*, muscles) involves complex mechanisms, and the rate constants k_p for clearance cannot be estimated accurately.

3.4. Recommendations

The rate constants for clearance calculated in our study may be applied in PBPK models for nanomedicine research and NP risk assessment. To increase the application domain for more NPs, we explored options for linking clearance to NP size and surface coating. Nevertheless, several limitations should be noted in the present study. First, our study did not consider aggregation and protein modification. Secondly, our generic model only involved size as the only variable, while the expanded model requires specific information on single types of surface coatings. Characterization of NPs with mixed coatings[60] need more methods to define in the future. Thirdly, the model application to soluble NPs (*e.g.*, ZnO and AgNPs)[103] requires combining properties of NPs and ions. Fourthly, our dataset only included spherical NPs with administration by intravenous injection due to limited data. Lastly, we limited ourselves to NPs because data on microparticles (MPs) are lacking and theories on NPs may not apply to MPs due to the greater gravity or resistance.[41] In the future, we will therefore focus on addressing these limitations.

4. Conclusions

The data on clearance of NPs from blood after intravenous injection generally fit one- and two-compartment kinetics. The generic model (NP size-based) was used to estimate rate constants for clearance obtained by one-compartment kinetics following pore penetration and phagocytosis pathways. Hydrodynamic diameter ~20 nm is reported as the optimal size for fast clearance of NPs from blood in the current dataset. The effect of surface coatings on clearance rate constants k_c based on two-compartment kinetics can be explained by an extended model (NP size- and surface coating-based), combining properties of NPs (size and surface coatings) and macrophages. These models may provide basic approaches to increase the application domain of PBPK models for the design of NPs in drug delivery or assessing the biological hazards of NPs.

Conflicts of interest

The authors declare no conflict of interest.

Acknowledgements

We would like to express our gratitude to the China Scholarship Council for the support of the first author at Radboud University Nijmegen.

References

1 R. Lopez-Cabeza, M. Kah, R. Grillo, M. Koutny, J. Salac, Z. Bilkova, M. Eghbalinejad and J. Hofman, Tebuconazole and terbuthylazine encapsulated in nanocarriers: preparation, characterization and release kinetics, *Environ. Sci.: Nano*, 2022, **9**, 1427–1438.
2 D. Peng, Y. Du, Y. W. Shi, D. Mao, X. H. Jia, H. Li, Y. K. Zhu, K. Wang and J. Tian, Precise diagnosis in different scenarios using photoacoustic and fluorescence imaging with dual-modality nanoparticles, *Nanoscale*, 2016, **8**, 14480–14488.
3 M. Goel, Y. Mackeyev and S. Krishnan, Radiolabeled nanomaterial for cancer diagnostics and therapeutics: principles and concepts, *Cancer Nanotechnol.*, 2023, **14**, 15.
4 J. J. Shi, P. W. Kantoff, R. Wooster and O. C. Farokhzad, Cancer nanomedicine: progress, challenges and opportunities, *Nat. Rev. Cancer*, 2017, **17**, 20–37.
5 A. Truskewycz, H. Yin, N. Halberg, D. T. H. Lai, A. S. Ball, V. K. Truong, A. M. Rybicka and I. Cole, Carbon Dot Therapeutic Platforms: Administration, Distribution, Metabolism, Excretion, Toxicity, and Therapeutic Potential, *Small*, 2022, **18**, e2106342.

6 P. Kocbek, K. Teskac, M. E. Kreft and J. Kristl, Toxicological Aspects of Long-Term Treatment of Keratinocytes with ZnO and TiO2 Nanoparticles, *Small*, 2010, **6**, 1908–1917.
7 A. S. Anand, K. Jain, A. Chauhan, D. N. Prasad and E. Kohli, Zinc oxide nanoparticles trigger dysfunction of mitochondrial respiratory complexes and repair dynamics in human alveolar cells, *Toxicol. Ind. Health*, 2023, **39**, 127–137.
8 A. Shimada, N. Kawamura, M. Okajima, T. Kaewamatawong, H. Inoue and T. Morita, Translocation pathway of the intratracheally instilled ultrafine particles from the lung into the blood circulation in the mouse, *Toxicol. Pathol.*, 2006, **34**, 949–957.
9 Y. Pan, S. Neuss, A. Leifert, M. Fischler, F. Wen, U. Simon, G. Schmid, W. Brandau and W. Jahnen-Dechent, Size-dependent cytotoxicity of gold nanoparticles, *Small*, 2007, **3**, 1941–1949.
10 W. H. De Jong and P. J. A. Borm, Drug delivery and nanoparticles: Applications and hazards, *Int. J. Nanomed.*, 2008, **3**, 133–149.
11 M. W. Wang, P. Zhang, Z. Y. Li, Y. Yan, X. Cheng, G. Wang and X. S. Yang, Different cellular mechanisms from low- and high-dose zinc oxide nanoparticles-induced heart tube malformation during embryogenesis, *Nanotoxicology*, 2022, **16**, 580–596.
12 F. A. Monikh, M. G. Vijver, R. Kortet, I. Lynch and W. Peijnenburg, Emerging investigator series: perspectives on toxicokinetics of nanoscale plastic debris in organisms, *Environ. Sci.: Nano*, 2022, **9**, 1566–1577.
13 M. Kumar, P. Kulkarni, S. F. Liu, N. Chemuturi and D. K. Shah, Nanoparticle biodistribution coefficients: A quantitative approach for understanding the tissue distribution of nanoparticles, *Adv. Drug Delivery Rev.*, 2023, **194**, 114708.
14 D. P. K. Lankveld, A. G. Oomen, P. Krystek, A. Neigh, A. Troost-de Jong, C. W. Noorlander, J. C. H. Van Eijkeren, R. E. Geertsma and W. H. De Jong, The kinetics of the tissue distribution of silver nanoparticles of different sizes, *Biomaterials*, 2010, **31**, 8350–8361.
15 Z. M. Lin, N. A. Monteiro-Riviere and J. E. Riviere, A physiologically based pharmacokinetic model for polyethylene glycol-coated gold nanoparticles of different sizes in adult mice, *Nanotoxicology*, 2016, **10**, 162–172.
16 V. V. Kasyanova and I. N. Bazhukova, Modeling of cerium oxide nanoparticles pharmacokinetics, *AIP Conf. Proc.*, 2020, **2313**, 080015.
17 G. Bachler, N. von Goetz and K. Hungerbuhler, Using physiologically based pharmacokinetic (PBPK) modeling for dietary risk assessment of titanium dioxide (TiO2) nanoparticles, *Nanotoxicology*, 2015, **9**, 373–380.
18 W. Y. Chen, Y. H. Cheng, N. H. Hsieh, B. C. Wu, W. C. Chou, C. C. Ho, J. K. Chen, C. M. Liao and P. Lin, Physiologically based pharmacokinetic modeling of zinc oxide nanoparticles and zinc nitrate in mice, *Int. J. Nanomed.*, 2015, **10**, 6277–6292.
19 A. R. R. Pery, C. Brochot, P. H. M. Hoet, A. Nemmar and F. Y. Bois, Development of a physiologically based kinetic model for 99m-Technetium-labelled carbon nanoparticles inhaled by humans, *Inhalation Toxicol.*, 2009, **21**, 1099–1107.
20 H. A. Lee, T. L. Leavens, S. E. Mason, N. A. Monteiro-Riviere and J. E. Riviere, Comparison of Quantum Dot Biodistribution with a Blood-Flow-Limited Physiologically Based Pharmacokinetic Model, *Nano Lett.*, 2009, **9**, 794–799.
21 L. Kagan, P. Gershkovich, K. M. Wasan and D. E. Mager, Dual Physiologically Based Pharmacokinetic Model of Liposomal and Nonliposomal Amphotericin B Disposition, *Pharm. Res.*, 2014, **31**, 35–45.
22 M. G. Li, Z. Panagi, K. Avgoustakis and J. Reineke, Physiologically based pharmacokinetic modeling of PLGA nanoparticles with varied mPEG content, *Int. J. Nanomed.*, 2012, **7**, 1345–1356.
23 D. Dong, X. Wang, H. L. Wang, X. W. Zhang, Y. F. Wang and B. J. Wu, Elucidating the in vivo fate of nanocrystals using a physiologically based pharmacokinetic model: a case study with the anticancer agent SNX-2112, *Int. J. Nanomed.*, 2015, **10**, 2521–2535.
24 D. S. Li, G. Johanson, C. Emond, U. Carlander, M. Philbert and O. Jolliet, Physiologically based pharmacokinetic modeling of polyethylene glycol-coated polyacrylamide nanoparticles in rats, *Nanotoxicology*, 2014, **8**, 128–137.
25 X. W. Liang, H. L. Wang, J. E. Grice, L. Li, X. Liu, Z. P. Xu and M. S. Roberts, Physiologically Based Pharmacokinetic Model for Long-Circulating Inorganic Nanoparticles, *Nano Lett.*, 2016, **16**, 939–945.
26 W. C. Chou, Y. H. Cheng, J. E. Riviere, N. A. Monteiro-Riviere, W. G. Kreyling and Z. M. Lin, Development of a multi-route physiologically based pharmacokinetic (PBPK) model for nanomaterials: a comparison between a traditional versus a new route-specific approach using gold nanoparticles in rats, *Part. Fibre Toxicol.*, 2022, **19**, 47.
27 B. Q. Lu, A. J. Hendriks and T. M. Nolte, A generic model based on the properties of nanoparticles and cells for predicting cellular uptake, *Colloids Surf., B*, 2022, **209**, 112155.
28 A. Nacev, C. Beni, O. Bruno and B. Shapiro, The behaviors of ferromagnetic nano-particles in and around blood vessels under applied magnetic fields, *J. Magn. Magn. Mater.*, 2011, **323**, 651–668.
29 S. Seo, H. Kim, J. H. Sung, N. Choi, K. Lee and H. N. Kim, Microphysiological systems for recapitulating physiology and function of blood-brain barrier, *Biomaterials*, 2020, **232**, 119732.
30 Y. H. Kim, K. J. Kim, D. Z. D'Argenio and E. D. Crandall, Characteristics of Passive Solute Transport across Primary Rat Alveolar Epithelial Cell Monolayers, *Membranes*, 2021, **11**, 331.
31 E. Gagliardini, S. Conti, A. Benigni, G. Remuzzi and A. Remuzzi, Imaging of the Porous Ultrastructure of the Glomerular Epithelial Filtration Slit, *J. Am. Soc. Nephrol.*, 2010, **21**, 2081–2089.
32 H. Sarin, Physiologic upper limits of pore size of different blood capillary types and another perspective on the dual pore theory of microvascular permeability, *Vasc. Cell*, 2010, **2**, 14.

33 S. M. Moghimi, A. C. Hunter and T. L. Andresen, Factors Controlling Nanoparticle Pharmacokinetics: An Integrated Analysis and Perspective, *Annu. Rev. Pharmacol. Toxicol.*, 2012, **52**, 481–503.
34 W. Poon, Y. N. Zhang, B. Ouyang, B. R. Kingston, J. L. Y. Wu, S. Wilhelm and W. C. W. Chan, Elimination Pathways of Nanoparticles, *ACS Nano*, 2019, **13**, 5785–5798.
35 Y. Liu, W. Huang, C. F. Xiong, Y. X. Huang, B. J. Chen, L. Racioppi, N. Chao and T. Vo-Dinh, Biodistribution and sensitive tracking of immune cells with plasmonic gold nanostars, *Int. J. Nanomed.*, 2019, **14**, 3403–3411.
36 T. M. Nolte, B. Q. Lu and A. J. Hendriks, Nanoparticles in bodily tissues: predicting their equilibrium distributions, *Environ. Sci.: Nano*, 2023, **10**, 424–439.
37 B. Wang, X. He, Z. Y. Zhang, Y. L. Zhao and W. Y. Feng, Metabolism of Nanomaterials in Vivo: Blood Circulation and Organ Clearance, *Acc. Chem. Res.*, 2013, **46**, 761–769.
38 S. D. Li and L. Huang, Pharmacokinetics and biodistribution of nanoparticles, *Mol. Pharmaceutics*, 2008, **5**, 496–504.
39 K. Kettler, K. Veltman, D. van de Meent, A. van Wezel and A. J. Hendriks, Cellular uptake of nanoparticles as determined by particle properties, experimental conditions, and cell type, *Environ. Toxicol. Chem.*, 2014, **33**, 481–492.
40 J. Malaczewska, Impact of noble metal nanoparticles on the immune system of animals, *Med. Weter.*, 2014, **70**, 204–208.
41 X. P. Duan and Y. P. Li, Physicochemical Characteristics of Nanoparticles Affect Circulation, Biodistribution, Cellular Internalization, and Trafficking, *Small*, 2013, **9**, 1521–1532.
42 P. Decuzzi, B. Godin, T. Tanaka, S. Y. Lee, C. Chiappini, X. Liu and M. Ferrari, Size and shape effects in the biodistribution of intravascularly injected particles, *J. Controlled Release*, 2010, **141**, 320–327.
43 H. L. Qian, K. Wang, M. T. Lv, C. S. Zhao, H. Wang, S. C. Wen, D. C. Huang, W. Chen and Y. A. Zhong, Recent advances on next generation of polyzwitterion-based nanovectors for targeted drug delivery, *J. Controlled Release*, 2022, **343**, 492–505.
44 P. Aggarwal, J. B. Hall, C. B. McLeland, M. A. Dobrovolskaia and S. E. McNeil, Nanoparticle interaction with plasma proteins as it relates to particle biodistribution, biocompatibility and therapeutic efficacy, *Adv. Drug Delivery Rev.*, 2009, **61**, 428–437.
45 D. E. Owens and N. A. Peppas, Opsonization, biodistribution, and pharmacokinetics of polymeric nanoparticles, *Int. J. Pharm.*, 2006, **307**, 93–102.
46 G. Storm, S. O. Belliot, T. Daemen and D. D. Lasic, Surface modification of nanoparticles to oppose uptake by the mononuclear phagocyte system, *Adv. Drug Delivery Rev.*, 1995, **17**, 31–48.
47 N. Hoshyar, S. Gray, H. B. Han and G. Bao, The effect of nanoparticle size on in vivo pharmacokinetics and cellular interaction, *Nanomedicine*, 2016, **11**, 673–692.
48 B. Q. Lu, J. Q. Wang, P. T. J. Scheepers, A. J. Hendriks and T. M. Nolte, Generic prediction of exocytosis rate constants by size-based surface energies of nanoparticles and cells, *Sci. Rep.*, 2022, **12**, 17813.
49 E. Yaghini, E. Tacconi, A. Pilling, P. Rahman, J. Broughton, I. Naasani, M. R. S. Keshtgar, A. J. MacRobert and O. Della Pasqua, Population pharmacokinetic modelling of indium-based quantum dot nanoparticles: preclinical in vivo studies, *Eur. J. Pharm. Sci.*, 2021, **157**, 105639.
50 D. E. Mager, V. Mody, C. Xu, A. Forrest, W. G. Lesniak, S. S. Nigavekar, M. T. Kariapper, L. Minc, M. K. Khan and L. P. Balogh, Physiologically Based Pharmacokinetic Model for Composite Nanodevices: Effect of Charge and Size on In Vivo Disposition, *Pharm. Res.*, 2012, **29**, 2534–2542.
51 Y. B. Han, T. T. Wang, H. H. Liu, S. H. Zhang, H. Zhang, M. T. Li, Q. Sun and Z. Li, The release and detection of copper ions from ultrasmall theranostic Cu2-xSe nanoparticles, *Nanoscale*, 2019, **11**, 11819–11829.
52 K. C. Nguyen, Y. Zhang, J. Todd, K. Kittle, D. Patry, D. Caldwell, M. Lalande, S. Smith, D. Parks, M. Navarro, A. Massarsky, T. W. Moon, W. G. Willmore and A. F. Tayabali, Biodistribution and Systemic Effects in Mice Following Intravenous Administration of Cadmium Telluride Quantum Dot Nanoparticles, *Chem. Res. Toxicol.*, 2019, **32**, 1491–1503.
53 F. Naz, V. Koul, A. Srivastava, Y. K. Gupta and A. K. Dinda, Biokinetics of ultrafine gold nanoparticles (AuNPs) relating to redistribution and urinary excretion: a long-term in vivo study, *J. Drug Targeting*, 2016, **24**, 720–729.
54 W. M. Xue, Y. Y. Liu, N. Zhang, Y. D. Yao, P. Ma, H. Y. Wen, S. P. Huang, Y. N. Luo and H. M. Fan, Effects of core size and PEG coating layer of iron oxide nanoparticles on the distribution and metabolism in mice, *Int. J. Nanomed.*, 2018, **13**, 5719–5731.
55 K. Avgoustakis, A. Beletsi, Z. Panagi, P. Klepetsanis, E. Livaniou, G. Evangelatos and D. S. Ithakissios, Effect of copolymer composition on the physicochemical characteristics, in vitro stability, and biodistribution of PLGA-mPEG nanoparticles, *Int. J. Pharm.*, 2003, **259**, 115–127.
56 Y. Wenger, R. J. Schneider, G. R. Reddy, R. Kopelman, O. Jolliet and M. A. Philbert, Tissue distribution and pharmacokinetics of stable polyacrylamide nanoparticles following intravenous injection in the rat, *Toxicol. Appl. Pharmacol.*, 2011, **251**, 181–190.
57 W. S. Cho, M. Cho, J. Jeong, M. Choi, B. S. Han, H. S. Shin, J. Hong, B. H. Chung, J. Jeong and M. H. Cho, Size-dependent tissue kinetics of PEG-coated gold nanoparticles, *Toxicol. Appl. Pharmacol.*, 2010, **245**, 116–123.
58 R. H. Yang, L. W. Chang, J. P. Wu, M. H. Tsai, H. J. Wang, Y. C. Kuo, T. K. Yeh, C. S. Yang and P. Lin, Persistent tissue kinetics and redistribution of nanoparticles, quantum dot 705, in mice: ICP-MS quantitative assessment, *Environ. Health Perspect.*, 2007, **115**, 1339–1343.
59 Arnida, M. M. Janát-Amsbury, A. Ray, C. M. Peterson and H. Ghandehari, Geometry and surface characteristics of gold nanoparticles influence their biodistribution and uptake by macrophages, *Eur. J. Pharm. Biopharm.*, 2011, **77**, 417–423.
60 X. S. Liu, H. Li, Y. J. Chen, Q. Jin, K. F. Ren and J. Ji, Mixed-Charge Nanoparticles for Long Circulation, Low

Reticuloendothelial System Clearance, and High Tumor Accumulation, *Adv. Healthcare Mater.*, 2014, **3**, 1439–1447.

61 G. D. Zhang, Z. Yang, W. Lu, R. Zhang, Q. Huang, M. Tian, L. Li, D. Liang and C. Li, Influence of anchoring ligands and particle size on the colloidal stability and in vivo biodistribution of polyethylene glycol-coated gold nanoparticles in tumor-xenografted mice, *Biomaterials*, 2009, **30**, 1928–1936.

62 A. L. Bailly, F. Correard, A. Popov, G. Tselikov, F. Chaspoul, R. Appay, A. Al-Kattan, A. V. Kabashin, D. Braguer and M. A. Esteve, In vivo evaluation of safety, biodistribution and pharmacokinetics of laser-synthesized gold nanoparticles, *Sci. Rep.*, 2019, **9**, 12890.

63 D. Z. Yang, L. Z. Feng, C. A. Dougherty, K. E. Luker, D. Q. Chen, M. A. Cauble, M. M. B. Holl, G. D. Luker, B. D. Ross, Z. Liu and H. Hong, In vivo targeting of metastatic breast cancer via tumor vasculature-specific nano-graphene oxide, *Biomaterials*, 2016, **104**, 361–371.

64 F. Chen, T. R. Nayak, S. Goel, H. F. Valdovinos, H. Hong, C. P. Theuer, T. E. Barnhart and W. B. Cai, In Vivo Tumor Vasculature Targeted PET/NIRF Imaging with TRC105(Fab)-Conjugated, Dual-Labeled Mesoporous Silica Nanoparticles, *Mol. Pharmaceutics*, 2014, **11**, 4007–4014.

65 F. Chen, H. Hong, S. X. Shi, S. Goel, H. F. Valdovinos, R. Hernandez, C. P. Theuer, T. E. Barnhart and W. B. Cai, Engineering of Hollow Mesoporous Silica Nanoparticles for Remarkably Enhanced Tumor Active Targeting Efficacy, *Sci. Rep.*, 2014, **4**, 5080.

66 M. Benezra, O. Penate-Medina, P. B. Zanzonico, D. Schaer, H. Ow, A. Burns, E. DeStanchina, V. Longo, E. Herz, S. Iyer, J. Wolchok, S. M. Larson, U. Wiesner and M. S. Bradbury, Multimodal silica nanoparticles are effective cancer-targeted probes in a model of human melanoma, *J. Clin. Invest.*, 2011, **121**, 2768–2780.

67 Z. Z. Sun, M. Worden, J. A. Thliveris, S. Hombach-Klonisch, T. Klonisch, J. van Lierop, T. Hegmann and D. W. Miller, Biodistribution of negatively charged iron oxide nanoparticles (IONPs) in mice and enhanced brain delivery using lysophosphatidic acid (LPA), *Nanomedicine*, 2016, **12**, 1775–1784.

68 X. Q. Shan, C. S. Liu, Y. Yuan, F. Xu, X. Y. Tao, Y. Sheng and H. J. Zhou, In vitro macrophage uptake and in vivo biodistribution of long-circulation nanoparticles with poly(ethylene-glycol)-modified PLA (BAB type) triblock copolymer, *Colloids Surf., B*, 2009, **72**, 303–311.

69 Y. R. Duan, J. P. Xu, Y. Z. Lin, H. Yu, T. Gong, Y. G. Li and Z. R. Zhang, A preliminary study on MeO-PEG-PLGA-PEG-OMe nanoparticles as intravenous carriers, *J. Biomed. Mater. Res., Part A*, 2008, **87**, 515–523.

70 Z. Liu, Z. H. Li, J. H. Liu, S. Gu, Q. H. Yuan, J. S. Ren and X. G. Qu, Long-circulating Er^{3+}-doped Yb_2O_3 up-conversion nanoparticle as an in vivo X-Ray CT imaging contrast agent, *Biomaterials*, 2012, **33**, 6748–6757.

71 M. G. Vijver, Y. J. Zhai, Z. Wang and W. Peijnenburg, Emerging investigator series: the dynamics of particle size distributions need to be accounted for in bioavailability modelling of nanoparticles, *Environ. Sci.: Nano*, 2018, **5**, 2473–2481.

72 C. Y. Loo, E. L. Siew, P. M. Young, D. Traini and W. H. Lee, Toxicity of curcumin nanoparticles towards alveolar macrophage: Effects of surface charges, *Food Chem. Toxicol.*, 2022, **163**, 112976.

73 Z. L. Chen and Z. J. You, New expression for collision efficiency of spherical nanoparticles in Brownian coagulation, *J. Appl. Math. Mech.*, 2010, **31**, 851–860.

74 M. L. Eggersdorfer and S. E. Pratsinis, Agglomerates and aggregates of nanoparticles made in the gas phase, *Adv. Powder Technol.*, 2014, **25**, 71–90.

75 R. Arvidsson, S. Molander, B. A. Sandén and M. Hassellöv, Challenges in Exposure Modeling of Nanoparticles in Aquatic Environments, *Hum. Ecol. Risk Assess.*, 2011, **17**, 245–262.

76 M. Farshbaf, H. Valizadeh, Y. Panahi, Y. Fatahi, M. W. Chen, A. Zarebkohan and H. L. Gao, The impact of protein corona on the biological behavior of targeting nanomedicines, *Int. J. Pharm.*, 2022, **614**, 121458.

77 **https://chem.libretexts.org/Bookshelves/Physical_and_Theoretical_Chemistry_Textbook_Maps/Supplemental_Modules_(Physical_and_Theoretical_Chemistry)/Kinetics/06%3A_Modeling_Reaction_Kinetics/6.01%3A_Collision_Theory/6.1.06%3A_The_Collision_Theory**, 2013.

78 M. Smoluchowski, Drei Vorträge über Diffusion, Brownsche Molekularbewegung und Koagulation von Kolloidteilchen, *Phys. Z.*, 1916, **17**, 557–585.

79 K. Cui, C. L. Ardell, N. P. Podolnikova and V. P. Yakubenko, Distinct Migratory Properties of M1, M2, and Resident Macrophages Are Regulated by alpha(D)beta(2) and alpha(M)beta(2) Integrin-Mediated Adhesion, *Front. Immunol.*, 2018, **9**, 2650.

80 B. B. Hong and A. Z. Panagiotopoulos, Molecular Dynamics Simulations of Silica Nanoparticles Grafted with Poly(ethylene oxide) Oligomer Chains, *J. Phys. Chem. B*, 2012, **116**, 2385–2395.

81 A. Darras, J. Fiscina, N. Vandewalle and G. Lumay, Relating Brownian motion to diffusion with superparamagnetic colloids, *Am. J. Phys.*, 2017, **85**, 265–270.

82 Y. Q. Qie, H. F. Yuan, C. A. von Roemeling, Y. X. Chen, X. J. Liu, K. D. Shih, J. A. Knight, H. W. Tun, R. E. Wharen, W. Jiang and B. Y. S. Kim, Surface modification of nanoparticles enables selective evasion of phagocytic clearance by distinct macrophage phenotypes, *Sci. Rep.*, 2016, **6**, 26269.

83 S. A. MacParland, K. M. Tsoi, B. Ouyang, X. Z. Ma, J. Manuel, A. Fawaz, M. A. Ostrowski, B. A. Alman, A. Zilman, W. C. W. Chan and I. D. McGilvray, Phenotype Determines Nanoparticle Uptake by Human Macrophages from Liver and Blood, *ACS Nano*, 2017, **11**, 2428–2443.

84 C. J. C. Van Oss, M. K. Chaudhury and R. J. Good, Interfacial Lifshitz-van der Waals and Polar Interactions in Macroscopic Systems, *Chem. Rev.*, 1988, **88**, 927–941.

85 R. E. Beck and J. S. Schultz, Hindrance of solute diffusion within membranes as measured with microporous

membranes of known pore geometry, *Biochim. Biophys. Acta*, 1972, **255**, 273–303.
86 C. D. Walkey, J. B. Olsen, H. B. Guo, A. Emili and W. C. W. Chan, Nanoparticle Size and Surface Chemistry Determine Serum Protein Adsorption and Macrophage Uptake, *J. Am. Chem. Soc.*, 2012, **134**, 2139–2147.
87 H. L. Gao and Q. He, The interaction of nanoparticles with plasma proteins and the consequent influence on nanoparticles behavior, *Expert Opin. Drug Delivery*, 2014, **11**, 409–420.
88 M. Longmire, P. L. Choyke and H. Kobayashi, Clearance properties of nano-sized particles and molecules as imaging agents: considerations and caveats, *Nanomedicine*, 2008, **3**, 703–717.
89 H. S. Choi, W. Liu, P. Misra, E. Tanaka, J. P. Zimmer, B. I. Ipe, M. G. Bawendi and J. V. Frangioni, Renal clearance of quantum dots, *Nat. Biotechnol.*, 2007, **25**, 1165–1170.
90 P. Nativo, I. A. Prior and M. Brust, Uptake and intracellular fate of surface-modified gold nanoparticles, *ACS Nano*, 2008, **2**, 1639–1644.
91 M. Kaasalainen, V. Aseyev, E. von Haartman, D. S. Karaman, E. Makila, H. Tenhu, J. Rosenholm and J. Salonen, Size, Stability, and Porosity of Mesoporous Nanoparticles Characterized with Light Scattering, *Nanoscale Res. Lett.*, 2017, **12**, 74.
92 V. M. Weiss, H. Lucas, T. Mueller, P. Chytil, T. Etrych, T. Naolou, J. Kressler and K. Mäder, Intended and Unintended Targeting of Polymeric Nanocarriers: The Case of Modified Poly(glycerol adipate) Nanoparticles, *Macromol. Biosci.*, 2018, **18**, 1700240.
93 M. Lindén, Chapter Seven - Biodistribution and Excretion of Intravenously Injected Mesoporous Silica Nanoparticles: Implications for Drug Delivery Efficiency and Safety, *Enzymes*, 2018, **43**, 155–180.
94 D. Ye, M. N. Raghnaill, M. Bramini, E. Mahon, C. Aberg, A. Salvati and K. A. Dawson, Nanoparticle accumulation and transcytosis in brain endothelial cell layers, *Nanoscale*, 2013, **5**, 11153–11165.
95 F. Li, S. M. Li, A. El Ghzaoui, H. Nouailhas and R. X. Zhuo, Synthesis and gelation properties of PEG-PLA-PEG triblock copolymers obtained by coupling monohydroxylated PEG-PLA with adipoyl chloride, *Langmuir*, 2007, **23**, 2778–2783.
96 N. Kotagiri, J. Sakon, H. Han, V. P. Zharov and J. W. Kim, Fluorescent ampicillin analogues as multifunctional disguising agents against opsonization, *Nanoscale*, 2016, **8**, 12658–12667.
97 Y. T. Konttinen, J. Pajarinen, Y. Takakubo, J. Gallo, C. Nich, M. Takagi and S. B. Goodman, Macrophage Polarization and Activation in Response to Implant Debris: Influence by "Particle Disease" and "Ion Disease", *J. Long-Term Eff. Med. Implants*, 2014, **24**, 267–281.
98 M. W. Cole and D. Velegol, Van der Waals energy of a 1-dimensional lattice, *Mol. Phys.*, 2008, **106**, 1587–1596.
99 V. N. Shukla, A. K. Mehata, A. Setia, P. Kumari, S. K. Mahto, M. S. Muthu and S. K. Mishra, Rational design of surface engineered albumin nanoparticles of asiatic acid for EGFR targeted delivery to lung cancer: Formulation development and pharmacokinetics, *Colloids Surf., A*, 2023, **676**, 132188.
100 L. Wang, N. Hartel, K. X. Ren, N. A. Graham and N. Malmstadt, Effect of protein corona on nanoparticle-plasma membrane and nanoparticle-biomimetic membrane interactions, *Environ. Sci.: Nano*, 2020, **7**, 963–974.
101 S. H. Wang and E. E. Dormidontova, Selectivity of Ligand-Receptor Interactions between Nanoparticle and Cell Surfaces, *Phys. Rev. Lett.*, 2012, **109**, 238102.
102 C. Schleh, M. Semmler-Behnke, J. Lipka, A. Wenk, S. Hirn, M. Schaffler, G. Schmid, U. Simon and W. G. Kreyling, Size and surface charge of gold nanoparticles determine absorption across intestinal barriers and accumulation in secondary target organs after oral administration, *Nanotoxicology*, 2012, **6**, 36–46.
103 L. Yang, H. J. Kuang, W. Y. Zhang, Z. P. Aguilar, H. Wei and H. Y. Xu, Comparisons of the biodistribution and toxicological examinations after repeated intravenous administration of silver and gold nanoparticles in mice, *Sci. Rep.*, 2017, **7**, 3303.